Chiral-selective Plasmonic Metasurface Absorber Based on Bilayer Fourfold Twisted Semicircle Nanostructure at Optical Frequency

Yongzhi Cheng (chengyz@wust.edu.cn)
Wuhan Univsersity of Science and Technology https://orcid.org/0000-0003-4928-9872
Fu Chen
Wuhan University of Science and Technology
Hui Luo
Wuhan University of Science and Technology

Nano Express

Keywords: Circular dichroism, chiral selective absorption, twisted-semicircle nanostructure, plasmonic metasurface absorber

Posted Date: September 3rd, 2020

DOI: https://doi.org/10.21203/rs.3.rs-70454/v1

Version of Record: A version of this preprint was published on January 14th, 2021. See the published version at https://doi.org/10.1186/s11671-021-03474-6.

Abstract

In this paper, we demonstrate theoretically a plasmonic metasurface absorber (PMSA) for the high chiral-selective absorption for right-handed and left-handed circular polarization (RCP and LCP) lights at optical frequency. The PMSA is composed of a dielectric substrate sandwiched with bi-layer fourfold twisted semicircle nanostructure. Numerical simulation results that the proposed PMSA has a strong chiral selective absorption bands, where absorption peaks for LCP and RCP lights occur at different resonance frequencies resulting in significant circular dichroism (CD) effect. It is shown that the maximum absorbance of the PMSA can reach to 93.2% for LCP light and 91.6% for RCP light, and that the maximum CD magnitude is about 0.85 and 0.91 around 288.5 THz and 404 THz, respectively. The mechanism of the strong chiroptical response of the PMSA is illustrated and revealed by electric fields distributions. Furthermore, the influence of the geometry of the proposed PMSA on the chiral-selective absorption characterization is studied systematically. Due to the strong chiral-selective absorption and CD effect, the proposed PMSA can be found many potential applications in some areas, such as chiral imaging, optical filters, detecting, and optical communications.

PACS numbers: 42.25.Bs, 78.20.−e

1. Introduction

Chirality as a ubiquitous nature phenomenon refers to the geometric property of an object lacking any mirror plane or inversion symmetry, which will always remain relevant for science and technology [1, 2]. Chiral media usually appear in two enantiomeric forms, which are mirror symmetric and non-superposable on its mirror image by simple translation or rotation with differential optical response to left-handed and right-handed circular polarization (LCP and RCP) light [1]. Circular dichroism (CD) of circular polarization (CP) light is the most unique optical property induced by chiral media. CD effect refers to differential transmission or absorption of the RCP and LCP lights, which has a wide range of applications in biology, medical science, chemistry, as well as polarization related optoelectronic devices [3–5]. However, the CD effect of natural materials is extremely weak, which need to be enhanced significantly for practical application. Metasurfaces as a descendant of metamaterials that consist of a monolayer or few-layer planar nanostructures have shown great promise for arbitrary electromagnetic (EM) wave manipulation [6, 7]. In particular, chiral metasurface (CMS) as a sub-class of the metasurfaces is able to enhance the chiral optical effects by several orders of magnitude.

CMSs have gained tremendous interest since it can exhibit exotic EM properties including negative refractive index and optical activity [8, 9], asymmetric transmission [10, 11], giant CD effect [12–14], polarization conversion [15, 16], and wave front manipulation [17, 18]. Since then, various CMSs structures (such as split-ring, gammadion, spiral wire, L-shaped and so on) have been designed to achieve highly-efficient selective chiral field enhancement for LCP or RCP light as well as CD effect [19–30]. However, most of these CMS focus on the performance of chirality in transmission, while much less attention has been paid to the one in reflection/absorption for CP lights, which are equally important in

optical engineering. It is well known that the most previous absorbers are applied to linear polarization light, and such designs for CP lights are rarely studied. In fact, CMSs also could be used to construct novel chiral-selective absorbers for CP lights [22, 23, 26–30]. For instance, Li et al proposed an ultra-thin chiral-selective absorber based on the L-shaped folded metallic wires, which can only absorb the LCP wave in microwave region [22]. Wang et al demonstrated that chiral metamirror can almost perfectly reflect all the LCP light, while totally absorbing the RCP light in infrared region [26]. Tang et al proposed a chiral-selective plasmonic absorber based on η-shaped-resonators in visible, which can chiral-selective absorption as well as giant CD effect [27]. Then, near-infrared chiral plasmonic metasurface absorbers have been proposed and demonstrated to selectively absorb LCP or RCP light. However, the chiral-selective absorption level of the most CSMs is less than 90%. Thus, the effective design of the chiral-selective plasmonic metasurface absorber (PMSA) with the high chiral-selectivity absorption performance is highly desirable.

In this work, we present one kind of highly-efficient PMSA based on bilayer fourfold twisted-semicircle nanostructure working in near infrared and visible region. Such PMSA could selectively achieve over 90% absorption for different handed CP lights depending on the chirality at different resonance frequency. Due to the strong chiral-selective absorption of the proposed PMSA, a high CD value of about 0.9 can be realized accordingly. The physical mechanism behind chiral-selective absorption for different handed CP lights is analyzed in detail by electric field distributions. Furthermore, the effects of geometric parameters of the unit-cell on chiral-selective absorption are also studied systematically. This result can guide the design of PMSA with strong chiral-selective absorption and CD effect for many practical applications such as thermal absorber, optical communication devices, photodetector, optical filters, imaging and holograms.

2. Unit-cell Design And Simulation

Figure 1 present the schematic diagram of the proposed PMSA, which is made of a periodic array with unit-cell composed of bilayer fourfold twisted semicircle nanostructure separated by a dielectric substrate. The fourfold twisted semicircle nanostructure on each side of the dielectric substrate is positioned so that each one rotated by 90° with respect to its neighbor, and the bottom side each semicircle nanostructure is also rotated by 90° with respect to the top one, as shown in Fig. 1(b). Similarly to previous design [29], the top four semicircle nanostructures are connected with the bottom one by copper cylinders, and the radius of copper cylinder is the same with the semicircle wire width, which can increase conductive coupling. The twisted semicircle nanostructure can be viewed as a coupled resonator system, where the strong chiral responses arise from the electric and magneto inductive coupling between the two twisted connected semicircles. The conductive coupling can further increase the coupling strength [31, 32]. This simple twisted semicircle nanostructure with mirror symmetries are created in the top and bottom layers allowing the designed PMSA to enhance the chirality. The overall unit-cell of the proposed PMSA has a uniaxial fourfold rotational (C_4) symmetry for light propagation direction, not any mirror plane and center of inversion. The middle substrate layer is made of a loss-free

dielectric MgF_2 with relative permittivity of 1.9. The chiral metal nanostructures were selected as gold, and the material parameter is described by the Drude model [33]. The optimized geometric parameters of the unit-cell of the proposed PMSA are given as: p_x=p_y=600 nm, r= 70 nm, w= 40 nm, t_s=120 nm, t_m=30 nm. The unit-cell of the PMSA is periodic along the x- and y-axis directions with the periods of 600 nm to avoid diffraction under normal incidence light for frequencies up to 500 THz.

To verify its efficiency of the proposed PMSA, the full-wave EM simulations were performed based on the finite element method (FEM) by using the frequency domain solver in CST Microwave Studio. In simulation, the unit-cell boundary condition was applied along x- and y-axis direction and the two CP eigen lights were used directly. In simulation process, broadband CP lights are employed as the excitation sources and are normally through the unit-cell of the proposed PMSA from the -z to + z direction. Then, both transmission and reflection coefficients of both LCP and RCP lights can be obtained. Generally, the chiral-selective absorbance $A_-(\omega)/A_+(\omega)$ for the LCP/RCP light can be expressed using the equations [14, 29]: $A_-(\omega) = 1- R_{--}(\omega) - T_{--}(\omega) = 1- |r_{--}(\omega)|^2 - |t_{--}(\omega)|^2$, $A_+(\omega) = 1- R_{++}(\omega) - T_{++}(\omega) = 1- |r_{++}(\omega)|^2 - |t_{++}(\omega)|^2$, respectively. The $t_{--}(\omega)$ and $t_{++}(\omega)$ are the co-polarization transmission coefficients for LCP and RCP lights, while $r_{--}(\omega)$ and $r_{++}(\omega)$ are the co-polarization reflection coefficients, respectively. It should be noticed that the cross-polarization transmission coefficients ($t_{+-}(\omega)$, $t_{-+}(\omega)$) and reflection coefficients ($r_{+-}(\omega)$, $r_{-+}(\omega)$) for LCP and RCP lights are very small (< 0.01) due to the high C_4 symmetry of the unit-cell of the designed PMSA, thus negligible. In addition, CD effect is induced by the chiral-selective absorption of two CP lights, which can be expressed as [14, 29]:$\triangle = |t_{++}(\omega)| - |t_{--}(\omega)|$. The ellipticity and optical activity are also important parameters to measure the chirality of the designed chiral nanostructure. The ellipticity characterizes the polarization state of transmitted lights of the chiral structure, which is described by ellipticity angle $\eta = \arctan[(|t_{++}(\omega)| - |t_{--}(\omega)|) / (|t_{++}(\omega)| + |t_{--}(\omega)|)]$. While the optical activity characterizes the rotation property of polarization plane of a transmitted linear polarization light respect to the incident one, which is described by the polarization azimuth rotation angle $\theta = [\arg(t_{++}(\omega))-\arg(t_{--}(\omega))]/2$.

3. Results And Discussions

Figure 2(a) presents the simulated co-polarization transmission coefficients ($t_{++}(\omega)$, $t_{--}(\omega)$) and reflection coefficients ($r_{++}(\omega)$, $r_{--}(\omega)$) for normal incident LCP and RCP lights. Two chiral plasmonic resonance modes (mode 1 and mode 2) are evidently at frequencies of f_1 = 288.5 THz and f_2 = 404 THz, respectively. It can be observed that the co-polarization reflection coefficients ($r_{++}(\omega)$, $r_{--}(\omega)$) for LCP and RCP lights are equal; and both of them are less 0.4 across the whole interested frequency range. In addition, the magnitudes of $r_{++}(\omega)$ and $r_{--}(\omega)$ are decreased to about 0.15 around resonance frequencies, meaning that the relative impedance of the PMSA are nearly matched to free space for both RCP and LCP lights at resonances. It also can be seen that the co-polarization transmission coefficients ($t_{++}(\omega)$, $t_{--}(\omega)$) for RCP and LCP lights are different significantly at resoances due to the chiral nature of the proposed PMSA. Around the lower frequency point, the magnitude of $t_{++}(\omega)$ for the RCP light is about 0.93, which is much is only about 0.075. Around the higher

frequency point, the magnitude of $t_{--}(\omega)$ for the LCP light is decreased to minimal value of 0.018, while the one for the LCP is up to maximal value of about 0.92. It means that only the RCP light can be selected to pass through the PMSA while the LCP light is forbidden to transmit mostly at the lower frequency. While only the LCP light can be selected to pass through the PMSA while the RCP light is forbidden to transmit mostly at the higher frequency. This will cause the different distortion and absorption for the RCP and LCP lights going through the PMSA slab, implying a high efficiency chiral-selective absorption and giant CD effect at resonances.

Figure 2(b) shows the chiral-selective absorbance spectra ($A_+(\omega)$, $A_-(\omega)$) for both incident LCP and RCP lights. It can be observed that the chiral-selective absorbance for LCP and RCP lights is up to maximal value of about 93.2% and 91.6%, while the one for RCP and LCP lights is decreased to only about 8.7% and 4.8% around the above two resonances, respectively. Obviously, the designed PMSA has the high absorption level for an LCP light whereas the weak absorption for RCP light around the lower frequency. On the other hand, the PMSA becomes strongly absorptive for RCP light while quite weak absorption for LCP light around the higher frequency. It means a chiral-selective absorption for two CP lights with particular handedness while reflecting the other one at different resonance frequency. It is worth highlighting that the PMSA has the two chiral-selective strong absorption frequency band just using a single size chiral nanostructure, which is much superior compared with the previous chiral absorbers for one absorption required different size ones for each CP light [22, 23, 26, 28, 30, 34]. Thus, the designed chiral nanostructure can act serve as a perfect LCP light absorber at the lower frequency and perfect RCP light absorber at the higher frequency. The characteristic of high chiral-selective absorption for CP lights will result in a giant CD effect.

The chiral-selective absorption or transmission difference between the LCP and RCP lights can be characterized by CD parameter Δ. Figure 3(a) presents the CD spectrum of the PMSA, where the main peaks of CD parameter are about 0.85 and 0.91 at two selectively resonance frequencies, respectively; which is much greater than the current reported chiral nanostructures [14–28, 34–40]. The giant CD effect is caused by the strong chirality of the PMSA. Obviously, owing to the giant CD effect, the proposed PSMA can be applied as a transparent circular polarizer. To study its CP purity of the PSMA applied as a circular polarizer, we give the ellipticity angle η and polarization azimuth rotation angle θ as shwon in Fig. 3(b). It can be observed that the value of the η is about 40.4° and − 43.9°, while the one of the θ is about 0° at the lower and higher frequencies, respectively. It means that the transmitted lights exhibit prominent RCP and LCP characteristics after lights passing through the PMSA slab at the lower and higher frequencies, respectively. It should be noticed that this PMSA based circular polarizer with the higher CP purity is valid for any arbitrarily polarization lights due to its high C_4 symmetry of the unit-cell. Thus, the homogenous circular polarizer is realized with our prposed PMSA.

To fully understand the chiral-selective absorption and giant CD effect of the PMSA, we retrieved the refractive index Re(n), Re(n_-), Re(n_+) and chiral parameter Re(κ) using a standard retrieval procedure from the transmission and reflection coefficients of CP lights [41, 42], as shwon in Figs. 4(a) and (b). It is

clearly that there are two resonances related to the strong chirality for the designed PMSA. The lower frequency resonance occurs around 288.5 THz and the higher one happens around 404 THz, which are consistent with where the chiral-selective absorption and CD peaks. As shown in Fig. 4(a), the Re(n) is negative with maximal magnitudes of -2.3 and − 1.1, and the Re(κ) is up to maximal magnitudes of 6.4 and − 5.1 around above two resonance frequencies, respectively. It is clear that the chiral parameter κ also contributes to the negative refractive index of RCP and LCP lights. The strong chirality can easily push the refractive index of the RCP/LCP light to become negative at resonance frequencies due to the relation of $n_{\pm} = n \pm \kappa$. Thus, as shown in Fig. 4(b), the Re(n_-) for LCP light and Re(n_+) for RCP light is negative from 286.2 THz to 291 THz, and 400.2 THz to 404 THz, respectively. In addition, the Re(n_-) and Re(n_+) are up to the maximal negative values of -8.6 and − 6.3 at above two resonance frequencies, respectively. It reveals that the high chrial-selective absorption as well as giant CD effect of the proposed PMSA are associated with the negative refractive property of the LCP and RCP lights.

To further unveil the origin of the chiral-selective absorption associated with the giant CD effect of the proposed PMSA, we studied the electric field (E_z) distributions of the unit-cell driven by the incident RCP and LCP lights at 288.5 THz and 404 THz, respectively. The excitation of surface plasmons resonance will produce oscillating dipole fields due to the semicircle nanostructure with small diameters relative to the incident wavelength of the different CP lights [43–46]. When RCP or LCP light excites the semicircle nanostructure, a chiral-selective absorption and giant CD effect will occur, and the electric field and magnetic field components of each layer are different due to the chirality [46–51].

Figure 5 show the electric field (E_z) distributions of the proposed PMSA drived by RCP and LCP lights at different resonance frequencies. The detail plot of the electric field (E_z) distributions on the semicircle nanostructure clearly shows the nature of each sruface plasmonics mode. The red and blue region on the top and bottom layers of the semicircle nanostructure present the positive and negative charge accumulations provided under RCP and LCP light excitation. It can be seen that the positive and negative charges are separated and mainly accumulated at the corners of the each semicircle nanostructure, acting like an electric dipole. It can be observed that the electric dipole power is much more than the magnetic dipole power for the designed semicircle nanostructure, thus, the electric dipole oscillations are predominant. The chiral-selective absorption and giant CD effect will be generated at resonance frequencies owing to the obvious dipole power difference under LCP and RCP excitation. Here, we use a simplified method with equivalent electric dipole moments, which considers the charge vibrations of four semicircle nanostructure per layer to one dipole vibration [46–48]. According to Born-Kuhn theory model [48, 49], when the mode is hybridized from two dipoles with the same electric field direction, namely bonding mode, while the one is hybridized from two dipoles with 90° or cross direction, known as antibonding mode. As shown in Figs. 5(a1,b1), under RCP light at resonance frequency f_1 = 288.5 THz, the electric dipole fields in top and bottom layers shows the cross directions and form a antibonding mode based on the Born-Kuhn model, resulting in high transmission of RCP light. As shown in Figs. 5 (c1,d1), under LCP light, it can be seen that it is hybrid from the bonding mode between the upper and ctric dipole moments, resulting in high

absorption level of LCP light. Thus, at the lower frequency, the bonding and antibonding modes cause different resonance energy and thus different transmission and absorption of chiral nanostructures under LCP and RCP lights (See Fig. 2). As shown in Figs. 5(a2,b2) and (c2,d2), under RCP light and LCP lights at resonance frequency f_2 = 404 THz, the electric dipole fields in top and bottom layers shows the same and cross directions, and form bonding and antibonding modes, respectively; resulting in high absorption level for RCP light and high transmission for LCP light. Thus, it can be seen that two chiral-selective absorption and CD effect are mainly attributed to the bonding and antibonding modes induced by hybrid coupling of the top and bottom layer electric dipole moments.

In the following, we investigate the influences of the geometric parameters of the unit-cell on the chiral-selective absorption properties of the proposed PMSA. Figure 6 shows the simulated chiral-selective absorbance spectra for these different geometric parameters (r, w, t_m, and t_s) of the unit-cell. For the proposed chiral nanostructure, the parameter-depended chiral-selective absorbance will show some interesting spectral variation characteristics since the influence process is complex and multi-factor competitive. In this study, the geometric parameters of the control group are r = 70 nm, w = 40 nm, t_m=30 nm, and t_s=120 nm, and changing one parameter at a time.

The semicircle nanostructure with the different r (r = 65 nm, 70 nm, 75 nm, and 80 nm) were firstly calculated, while the other parameters are fixed. As shown in Fig. 6(a), when increasing r, the resonance frequencies for both LCP and RCP waves decrease gradually, which can be interpreted by the equivalent LC resonance circuit theory [52, 53]. The resonance frequencies for both LCP and RCP lights can be expressed as $f = \frac{1}{2\pi\sqrt{LC}}$, where equivalent capacitance C and inductance L are mainly determined by the geometric parameters of the proposed PMSA. The L will increase with the increase of the r, thus resulting in the decrease of the resonance frequencies. In addition, when increasing r, the absorbance of the LCP light will decrease gradually while the one of the RCP light will be nearly unchanged. Figure 6(b) shows the absorbance spectra of the LCP and RCP lights when changing the w from 30 nm to 45 nm by a step of 5 nm, while the other parameters are kept unchanged. It can be seen that the resonance frequencies for both LCP and RCP lights will increase gradually with the increase of the w. Obviously, the decrease of the resonance frequencies is mainly due to the increase of the C. The absorbance of the LCP light will firstly increase and the then decrease slightly, while the one of the RCP light will decrease gradually when increasing r. As shown in Fig. 6(c), we present the absorbance spectra of the LCP and RCP lights with varying t_m from 20 nm to 50 nm by a step of 10 nm and other parameters fixed. There are similar cases to the change of w, when increasing t_m, the resonance frequency for LCP light decrease significantly, and the one for RCP light decrease slightly. In this case, the L will decrease with the increasing of the t_m, thus resulting in the increase of the resonance frequencies. In addition, the absorbance of the LCP light will increase gradually, while the one of the RCP light will firstly increase and then decrease when increasing t_m. Finally, we present the absorbance spectra of the LCP and RCP lights with different t_s (t_s = 110 nm, 120 nm, 130 nm, and 140 nm), and other parameters are kept unchanged, as shown in Fig. 6(d). It can be observed that the resonance frequencies for both LCP and RCP lights decrease when increasing t_s. In this

case, the C will decrease when increasing t_s, thus resulting in the increase of the resonance frequencies. In addition, when increasing t_s, the absorbance of the LCP will increase gradually, while the one of the RCP light will decrease slightly. It can be concluded that the resonance frequencies and absorption level for both RCP and LCP lights are sensitive to the geometric parameters of the unit-cell of the designed PMSA. Thus, the chiral-selective absorption properties of the proposed PMSA can be adjusted dynamically by varying geometric parameters.

4. Conclusion

In conclusion, a PMSA based on a bi-layered fourfold twisted semicircle nanostructure is proposed to achieve near perfect chiral-selective absorption for RCP and LCP lights as well as giant CD effect in near near-infrared and visible region. The simulation results exhibit that the chiral-selective absorbance for both RCP and LCP lights are more than 90%, and the CD magnitude is up to 0.91. The retrieved effective EM parameters indicate that the lower frequency absorption and CD effect are associated with the negative refraction property of the LCP light, and the higher ones are to the RCP light. The electric field distributions indicate that the chiral-selective absorption properties and giant CD effect of the PMSA mainly originates from the bonding and antibonding modes induced by hybrid coupling of the top and bottom layer electric dipole moments. Furthermore, the resonance frequencies and chiral-selective absorption level of the PMSA can be tuned by changing the geometric parameters of the unit-cell. This design of the PMSA is promising for future applications in optical filter, chiral imaging, circular polarizer, detecting, and optical communications.

Declarations

Acknowledgements

We acknowledge the financial support from the National Natural Science Foundation of China (Grant Nos. 61701185, and 61801186) and the Science and Technology Research Project of Education Department of Hubei China (Grant No.D20181107).

References

1. Barron LD (2004) Molecular light scattering and optical activity. Cambridge University Press, Cambridge
2. Plum E, Zheludev NI (2015) Chiral mirrors. Appl Phys Lett 106(22):221901
3. Vassilios, Yannopapas (2009) Circular dichroism in planar nonchiral plasmonic metamaterials. Opt Lett 34(5):632–634
4. Wang BN, Zhou JF, Koschny T, Soukoulis CM (2009) Nonplanar chiral metamaterials with negative index. Appl Phys Lett 94:151112

5. Sharma V, Crne M, Park JO, Srinivasarao M (2009) Structural origin of circularly polarized iridescence in jeweled beetles. Science 325:449–451
6. Cheng H, Liu Z, Chen S, Tian J, "Emergent Functionality and Controllability in Few- Layer Metasurfaces," Advanced Materials, vol. 27, pp. 5410–5421, 2015
7. He Q, Sun S, Shiyi Xiao, and Zhou L, High-Effiiency Metasurfaces: Principles, Realizations, and Applications, Adv. Optical Mater. 2018, 1800415
8. Cole MA, Chen Wen-chen, Liu M, Kruk SS, Padilla WJ, Shadrivov IV, Powell DA (2017) Strong Broadband Terahertz Optical Activity through Control of the Blaschke Phase with Chiral Metasurfaces. Phys Rev Appl 8:014019
9. Chen HR, Cheng YZ, Zhao JC, Mao XS (2018) Multi-band terahertz chiral metasurface with giant optical activities and negative refractive index based on T-shaped resonators. Mod Phys Lett B Vol 32:1850366 No. 30)
10. Fedotov VA, Schwanecke AS, Zheludev NI, Khardikov VV, Prosvirnin SL (2007) Asymmetric transmission of light and enantiomerically sensitive plasmon resonance in planar chiral nanostructures. Nano Lett 7:1996–1999
11. De jun Liu, Zhong yin Xiao, Zi huaWang, Multi-Band Asymmetric Transmission and 90° Polarization Rotator Based on Bi-Layered Metasurface with F-Shaped Structure, Plasmonics (2017) 12:445–452
12. Zeng Wang BH, Teh Y, Wang G, Adamo J, Teng, Sun H (2017) Enhancing circular dichroism by super chiral hot spots from a chiral metasurface with apexes. Appl Phys Lett 110:221108
13. Zhang M, Lu Q, Zheng H (2018) Tunable circular dichroism created by surface plasmons in bilayer twisted tetramer nanostructure arrays. J Opt Soc Am B 35:689–693
14. Yongzhi Cheng Fu, Chen H, Luo (2020) Multi-band giant circular dichroism based on conjugated bilayer twisted-semicircle nanostructure at optical frequency. Phys Lett A 384:126398
15. Wu S, Xu Su, Zinenko TL, Yachin VV, Prosvirnin SL (2019) and Vladimir R. Tuz, 3D-printed chiral metasurface as a dichroic dual-band polarization converter. Opt Lett Vol 44(4):1056–1059
16. Li Y, Li Z, Liu Y, Kong Y, Huang L (2019) Broadband and highly efficient polarization conversion in infrared region using plasmonic metasurfaces. Opt Mater 98:109420
17. Li Z, Cai X, Tian Y, Liu J (2019) Shaping the wavefront of light with high-order and short-period mode metasurfaces. Opt Commun 449:53–56
18. Fan J, Cheng Y (2020) Broadband high-efficiency cross-polarization conversion and multi-functional wavefront manipulation based on chiral structure metasurface for terahertz wave. J Phys D: Appl Phys 53:025109
19. Zhao R, Zhang L, Zhou J, Koschny T, Soukoulis CM (2011) Conjugated gammadion chiral metamaterial with uniaxial optical activity and negative refractive index. Phys Rev B 83:035105–035105
20. Ma X, Huang C, Pu M, Hu C, Feng Q, Luo X (2012) Multi-band circular polarizer using planar spiral metamaterial structure. Opt Express 20(14):16050–16058

21. Cheng Y, Nie Y, Wu L, Gong RZ (2013) Giant circular dichroism and negative refractive index of chiral metamaterial based on split-ring resonators. Progress In Electromagnetics Research 138:421–432
22. Li MH, Guo LY, Dong JF, Yang HL (2014) An ultra-thin chiral metamaterial absorber with high selectivity for LCP and RCP waves. J Phys D 47(18):185102
23. Li W, Coppens ZJ, Besteiro LV, Wang W, Govorov AO, Valentine J (2015) Circularly polarized light detection with hot electrons in chiral plasmonic metamaterials. Nat Commun 6(1):8379
24. Shang X-J, Zhai X, Wang L-L, He M-D, Li Q, Luo X, Hui-Gao D (2017) "Asymmetric transmission and polarization conversion of linearly polarized waves with bilayer L-shaped metasurfaces." 2017. Appl Phys Express 10:052602
25. Chen Y, Gao J, Yang X (2018) Chiral metamaterials of plasmonic slanted nanoapertures with symmetry breaking. Nano Lett 18(1):520–527
26. Zuojia Wang H, Jia K, Yao W, Cai H, Chen Y, Liu (2016) Circular Dichroism Metamirrors with Near-Perfect Extinction. ACS Photonics 3(11):2096–2101
27. Tang B, Li ZY, Palacios E, Liu ZH, Butun S, Aydin K (2017) Chiral-selective plasmonic metasurface absorbers operating at visible frequencies. IEEE Photonics Technol Lett 29(3):295–298
28. Leixin Ouyang W, Wang D, Rosenmann DA, Czaplewski J, Gao, Yang X (2018) Near-infrared chiral plasmonic metasurface absorbers. Opt Express Vol 26:Issue 24, pp. 31484–31489
29. Yongzhi Cheng H, Chen J, Zhao X, Mao, Cheng Z (2018) Chiral metamaterial absorber with high selectivity for terahertz circular polarization waves. Opt Mater Express 8(5):1399–1409
30. Kong X-T, Khorashad LK, Wang Z (2018) Alexander O. Govorov, Photothermal Circular Dichroism Induced by Plasmon Resonances in Chiral Metamaterial Absorbers and Bolometers. Nano Lett 18(3):2001–2008
31. Cui Y, Kang L, Lan S, Rodrigues S, Cai W, “Giant chiral optical response from a twisted-arc metamaterial Nano Lett.,” vol. 14, pp. 1021–1025, 2014
32. Sun B, Yu Y (2018) Analysis of circular dichroism in chiral metamaterial at terahertz frequencies. J Phys D Appl Phys 52:025105
33. Ordal MA et al (1983) Optical properties of the metals Al, Co, Cu, Au, Fe, Pb, Ni, Pd, Pt, Ag, Ti, and W in the infrared and far infrared. Appl Opt 22:1099–1120
34. Yongzhi Cheng H, Chen J, Zhao X, Mao, Cheng Z (2018) Chiral metamaterial absorber with high selectivity for terahertz circular polarization waves. Opt Mater Express 8(5):1399–1409
35. Hu L, Tian X, Huang Y, Fang L, Fang Y (2016) Quantitatively analyzing the mechanism of giant circular dichroism in extrinsic plasmonic chiral nanostructures by tracking the interplay of electric and magnetic dipoles. Nanoscale 8:3720–3728
36. TianKun Wang,Tong, Fu Y, Chen Z, Zhang (2017) Circular dichroism of a tilted U-shaped nanostructure. Opt Lett 42(14):2842–2845
37. Wang F, Fu T, Wang Y, Zhang Yu, Zhang Z, Li, Wang (2018) Plasmonic circular dichroism of a tailed spatial cross-shaped nanostructure. Journal of Optical Technology Vol 85(2):88–92

38. Xiaoyu Feng Yu, Bai Z, Jing Yu, Qu T, Wang H, Ullah, Zhang Z (2019) Enhanced circular dichroism of tilted zigzag-shaped nanohole arrays. Appl Opt Vol 58(1):177–181
39. Qi J, Zhang M, Zhang Y, Han Q, Gao W, Wang Y (2019) Runcai Miao, and Jun Dong, Multiband circular dichroism from bilayer rotational F4 nanostructure arrays. Appl Opt Vol 58(2):479–484
40. Mohsen Rajaei J, Zeng M, Albooyeh M, Kamandi M, Hanifeh F, Capolino, Kumar H, Wickramasinghe (2019) Giant circular dichroism at visible frequencies enabled by plasmonic ramp-shaped nanostructures. ACS Photonics 6:924–931
41. Zhou J, Dong J, Wang B, Koschny T, Kafesaki M, Soukoulis CM, “Negative refractive index due to chirality,” *Phys. Rev. B*, Vol. 79, No. 12, 121104(4), 2009
42. Zhao R, Koschny Th, Soukoulis CM (2010) Chiral metamaterials: retrieval of the effective parameters with and without substrate. Opt Express 18:14553
43. Bohren CF, Huffman DR (1983) Absorption and scattering of light by small particles. Wiley, New York
44. Liu N, Kaiser S, Giessen H (2008) Magnetoinductive and electroinductive coupling in plasmonic metamaterial molecules. Adv Mater 20:4521–4525
45. Wang Y, Qin F, Yi Z, Chen X, Zhou Z, Yang H, Liao X, Tang Y, Yao W, Yi Y (2019) Effect of slit width on surface plasmon resonance. Results in Physics 15:102711
46. Hor YL, Phua WK, Eng Huat Khoo, Chirality Switching Via Rotation of Bilayer Fourfold Meta-Structure, Plasmonics (2017) 12:83–87
47. Na Liu H, Giessen (2010) Coupling Effects in Optical Metamaterials. Angew Chem Int Ed 49:9838–9852
48. Yin X, Schäferling M, Metzger B, Giessen H (2013) Interpreting chiral nanophotonic spectra: the plasmonic Born–Kuhn model. Nano Lett 13:6238–6243
49. Qi J, Zhang M, Zhang Y, Han Q, Gao W, Wang Y (2019) Runcai Miao, and Jun Dong, Multiband circular dichroism from bilayer rotational F4 nanostructure arrays. Appl Opt Vol 58(2):479–484
50. Qin F, Chen Z, Chen X, Yi Z, Yao W, Duan T, Wu P, Yang H, Li G, Yi Y (2020) A tunable triple-band near-infrared metamaterial absorber based on Au nano-cuboids Array. Nanomaterials 10(2):207
51. Luo J, Cheng Y, Gong Z, Wu K, Zhou Y, Chen HX, Gauthier M, Cheng Y, Liang J, Zou T (2020) Self-assembled peptide functionalized gold nanopolyhedrons with excellent chiral optical properties. Langmuir 36(2):600–608
52. Maeda M (1972) An analysis of gap in microstrip transmission lines. IEEE Trans Microw Teory Tech 20:390
53. Li W, Cheng Y (2020) Dual-band tunable terahertz perfect metamaterial absorber based on strontium titanate (STO) resonator structure. Opt Commun 462:125265

Figures

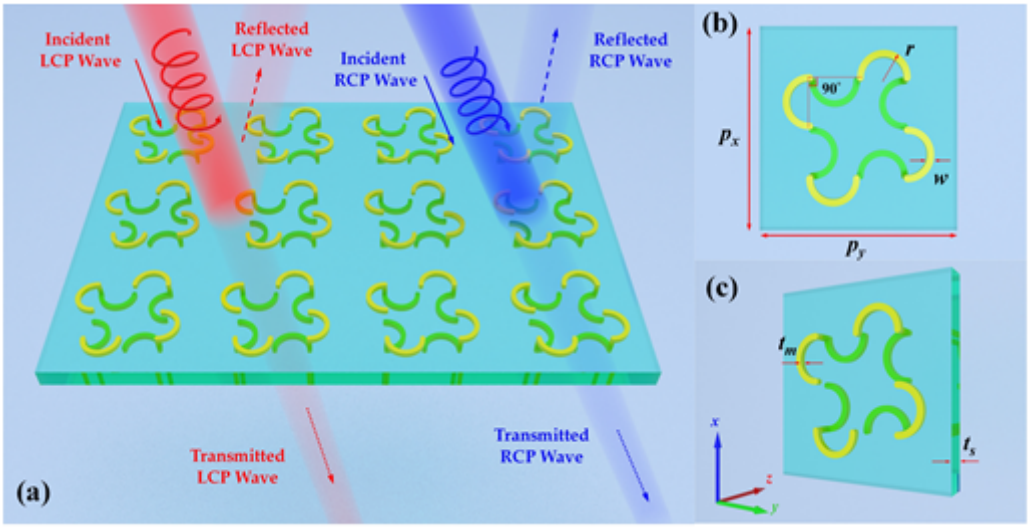

Figure 1

Schematic of the designed PMSA: (a) periodic array, (b-c) the front and perspective view of the unit-cell nanostructure.

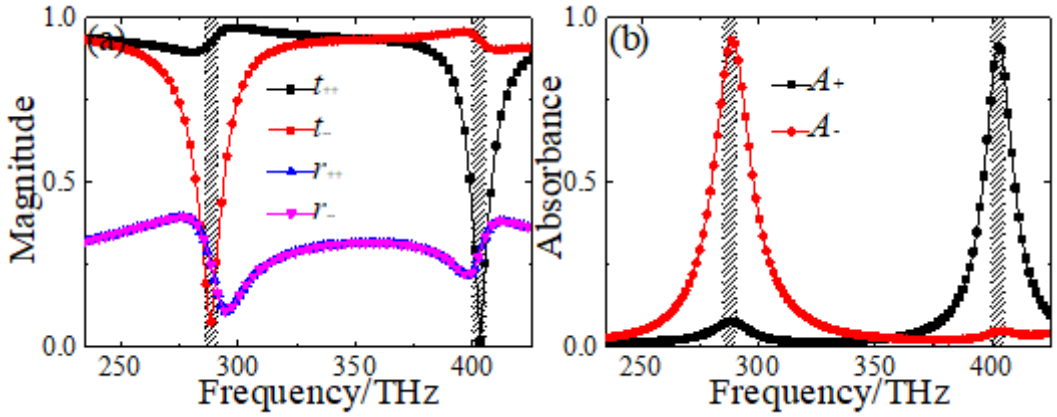

Figure 2

(a) Simulated co-polarization transmission coefficients (t++(ω), t–(ω)) and reflection coefficients (r++(ω), r–(ω)) for LCP and RCP lights, (b) the corresponding chiral-selective absorbance (A+(ω), A-(ω)) for LCP and RCP lights.

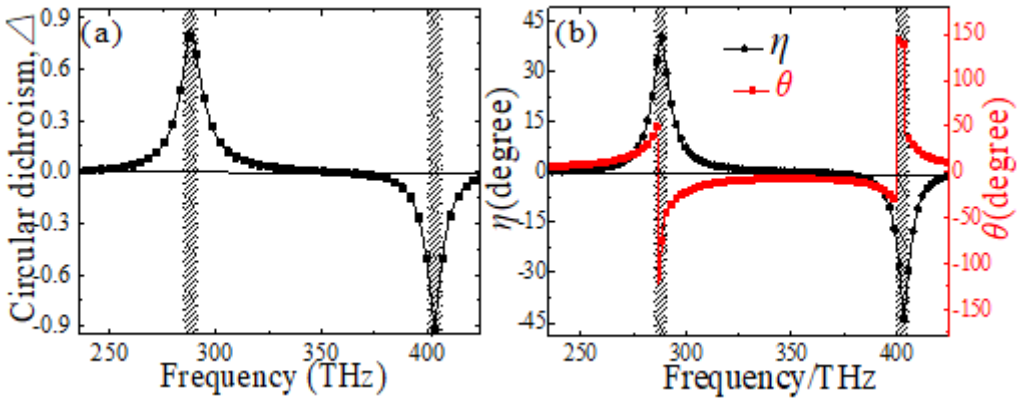

Figure 3

(a) The calculated CD parameter Δ, (b) ellipticity angle η and polarization azimuth rotation angle θ.

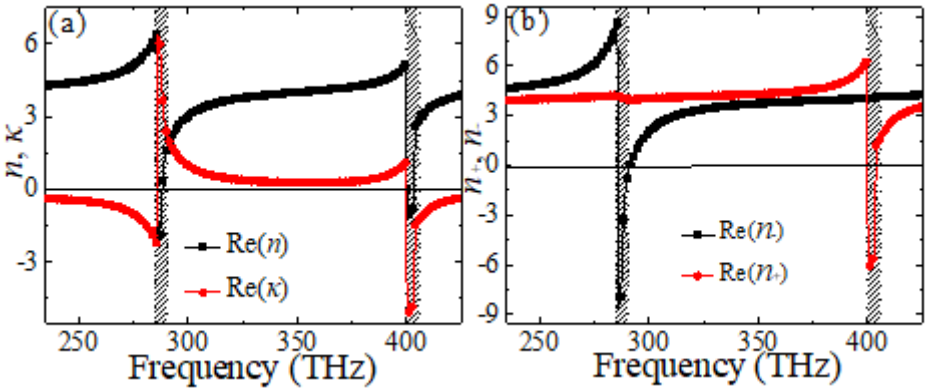

Figure 4

The retrieved real parts of (a) average refractive index Re(n) and chiral parameter Re(κ), (b) refractive index Re(n-), Re(n+) for LCP and RCP lights.

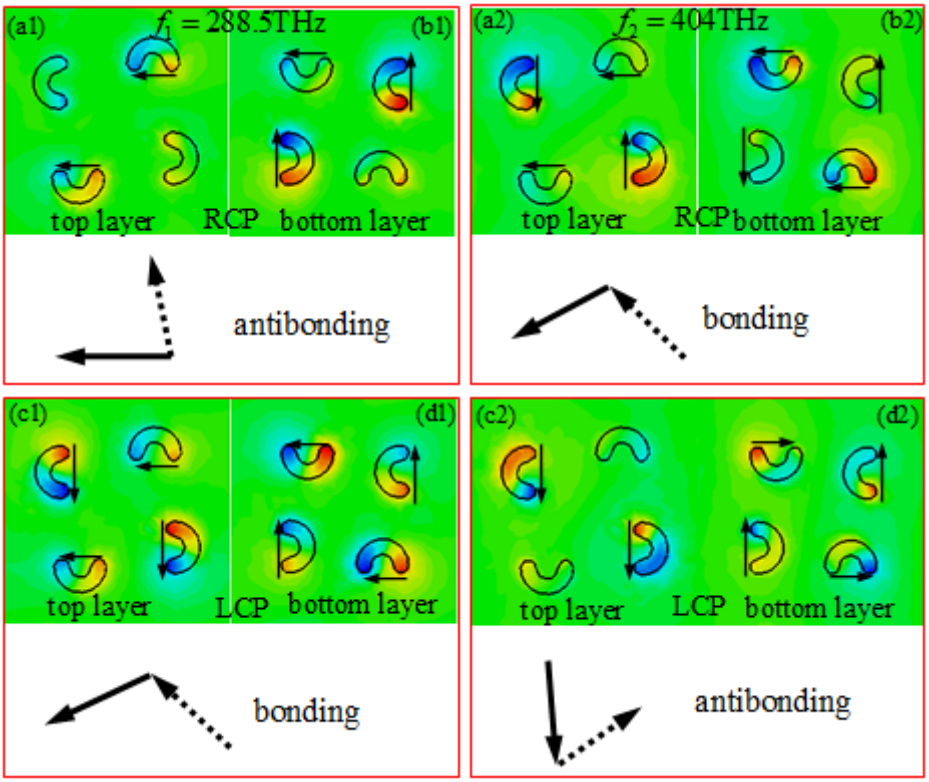

Figure 5

The electric field (Ez) distributions of unit-cell of the proposed PMSA induced by the (a1,b1,a2,b2) RCP and (c1,d1,c2,d2) LCP lights at different resonance frequencies: (a1-d1) f1 = 288.5 THz, (a2-d2) f2 = 404 THz. The black solid line (dash line) arrows denote the equivalent electric dipole moments on the top (bottom) layer of the proposed chiral nanostructure.

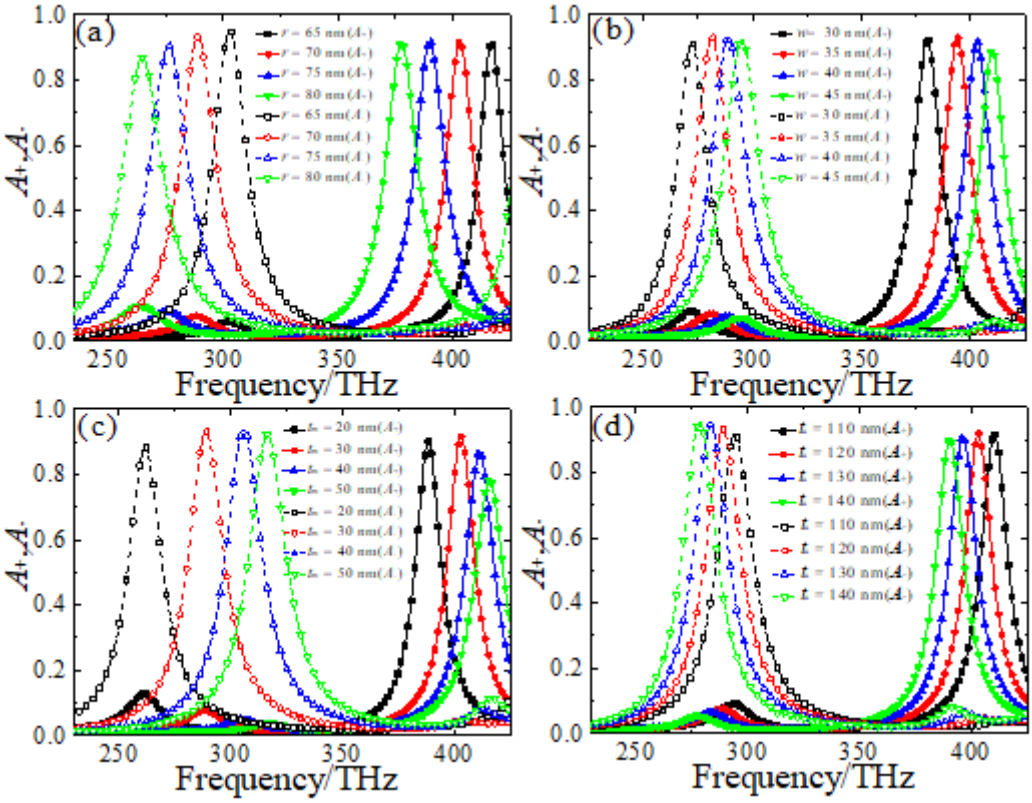

Figure 6

The simulated absorbance spectra of the LCP and RCP lights of proposed CMMA with different geometric parameters: (a-c) radius (r), wire width (w), and thickness (tm) of semicircle nanostructure, (d) thickness of dielectric substrate (ts).